Perfluorooctyl Bromide Traces Self-assembled with Polymeric Nanovesicles for Blood Pool Ultrasound Imaging

Journal:	*Biomaterials Science*
Manuscript ID	BM-ART-02-2016-000080.R1
Article Type:	Paper
Date Submitted by the Author:	18-Mar-2016

Complete List of Authors:	Li, Hao; South China Academy of Advanced Optoelectronics, South China Normal University, Institute of Electronic Paper Display; School of Chemistry and Chemical Engineering, Sun Yat-Sen University Wang, Ping; Sun Yat-Sen University, The Third Affiliated Hospital Wang, Xuan; Sun Yat-Sen University, School of Chemistry and Chemical Engineering Yin, Tinghui; Sun Yat-Sen University, The Third Affiliated Hospital zhou, guofu; South China Normal University, Institute of Electronic Paper Displays, South China Academy of Advanced Optoelectronics Shuai, Xintao; Sun Yat-Sen University, School of Chemistry and Chemical Engineering Zheng, Rongqin; Sun Yat-Sen University, The Third Affiliated Hospital

Biomaterials Science

ARTICLE

Perfluorooctyl bromide traces self-assembled with polymeric nanovesicles for blood pool ultrasound imaging

Received 00th January 20xx,
Accepted 00th January 20xx

DOI: 10.1039/x0xx00000x

www.rsc.org/

Hao Li,[a,b,†,*] Ping Wang,[c,†] Xuan Wang,[b] Tinghui Yin,[c] Guofu Zhou,[a] Xintao Shuai,[b,*] and Rongqin Zheng[c,*]

A novel perfluorooctyl bromide (PFOB)-loaded nanoveislce with the size of about 500 nm was prepared by self-assembly of amphiphilic block copolymer, poly(ethylene oxide)-b-poly(D,L-lactic acid) (PEG-PDLLA) for blood pool ultrasound imaging. The excellent compatibility of PFOB with hydrophobic PDLLA block makes PFOB uniformly distribute and integrate well within the nanovesicle shell. In theory, both the compressibility and shell density of nanovesicle as ultrasound scatterer are enhanced, resulting in much higher echo intensity than other PFOB nanoparticles. In vitro and in vivo imaging results illustrate that these polymeric nanovesicles with extremely low content of PFOB show quite good contrast-enhancing effect even if highly diluted in blood. So this PFOB-loaded polymeric nanovesicle is anticipated to be applicable as ultrasound contrast agent for normal angiography and specific imaging of capillary-abundant organs or tissues (e.g. tumor).

Introduction

Ultrasonography is the most extensively used imaging technique in clinical application, due to its safety, noninvasion, versatility, portability, low cost and real-time modality.[1] However, it's application is still limited due to the lack of imaging resolution and precision, especially for soft tissue where lesions are often hard to detect.[2] Many ultrasound contrast agents (UCA) represented by gas-filled microbubbles are developed to overcome such problems. In microbubbles, the encapsulated gas can greatly increase the acoustic impedance mismatch with ambient fluid (usually blood) to enhance back reflection for highlighting tissue borders.[2,3] Some of the microbubbles are commercially available, such as Levovist® (Schering AG), Optison® (Amersham), Definity® (Bristol-Myers Squibb), and Sonovue® (Braco).[4] However, their large sizes make them difficult to pass through capillary-abundant organs or tissues (e.g. tumor)[5], and their wide distribution of particle sizes is against accurate evaluation of pathological depth and extent.

[a] Institute of Electronic Paper Display, South China Academy of Advanced Optoelectronics, South China Normal University, Guangzhou 510006, P. R. China. Fax: +86 20 3931 4813; Tel: +86 20 3931 4813; E-mail: flyinghoyle@gmail.com
[b] School of Chemistry and Chemical Engineering, Sun Yat-Sen University, Guangzhou 510275, P. R. China. Fax: +86 20 8411 2245; Tel: +86 20 8411 0365; E-mail: shuaixt@mail.sysu.edu.cn
[c] Department of Ultrasonography, The Third Affiliated Hospital, Sun Yat-Sen University, Guangzhou 510630, P. R. China. Fax: +86 20 8753 6401; Tel: +86 20 8551 6867-3030; E-mail: zhengrongqin@hotmail.com
† These authors contributed equally to this work
Electronic Supplementary Information (ESI) available: [details of any supplementary information available should be included here]. See DOI: 10.1039/x0xx00000x

Nano-sized UCAs are promising solutions to such problems. One is gas-filled nanobubbles, but it is difficult to keep them stable in nanoscale unlike microbubbles.[6,7] Another is liquid fluorocarbon-loaded nanoemulsions or nanocapsules. For example, perfluorooctyl bromide [PFOB; boiling point (b.p.): 144 °C] appears to be a good content with high acoustic impedance mismatch based on its water immiscibility, high density and stability, and chemical and biological inertness.[8~12] Pisani et al. firstly prepared PFOB-filled nanocapsules modified with PEGylated phospholipid (DSPE-PEG) and poly(lactide-co-glycolide) (PLGA) to escape recognition and clearance by the mononuclear phagocyte system for passive tumor-targeting ultrasonic imaging.[8] Although phospholipid or surfactant-based hybrids greatly help the emulsification of liquid fluorocarbon, the interaction between phospholipid shell and fluorocarbon core is not strong enough to keep them stable in nanoscale. Recently, some amphiphilic block copolymers were adopted to replace phospholipid, surfactant and other emulsifiers for fabricating liquid fluorocarbon-loaded nanoemulsions or nanocapsules as UCAs.[13-17] Natalya Rapoport et al. prepared surface-stabilized nanoemulsions containing perfluoro-15-crown-5-ether in the aqueous phase for ultrasound-mediated tumor imaging, via self-assembly of poly(ethylene oxide)-b-poly(D,L-lactic acid) (PEG-PDLLA), poly(ethylene oxide)-b-poly(L-lactide) (PEG-PLLA), and poly (ethylene oxide)-b-poly(ε-caprolactone) (PEG-PCL).[17] Here the amphiphilic block copolymers can not only spontaneously form thermodynamically stable core-shell nanostructure encapsulating liquid fluorocarbon through the hydrophilic expanding and hydrophobic collapsing in aqueous solution, but also determine the size of the resulting nanoparticles well under certain preparation conditions.[17-19] Moreover polymer-coated

fluorocarbon nanodroplets also showed the increasing resistance to external pressure and the prolonging blood circulation time, besides the high stability and the size uniformity.[3]

After all, the most crucial feature of contrast-enhanced effect is the number of fluorocarbons in nanoemulsion or nanocapsule solution.[9] For some soft tissues or organs, even a minimal 40% volume concentration of PFOB is required for in vivo imaging.[20, 21] It is all but impossible to reach such high concentration of PFOB in previously reported nanodroplets. And the accumulation of too much PFOB may induce temporary obstacle of the reticular endothelial system and weaken the resistance to bacterial endotoxin.[22] In addition, given its high solubility of respiratory gases, excessive PFOB may also influence oxygen uptake of some normal cells.[23] Therefore, how to achieve reliable in vivo imaging under a low concentration of liquid fluorocarbon, especially blood pool imaging via intravenous injection, is still a challenge to these nanoemulsions or nanocapsules.

Polymeric vesicle is a hollow sphere that encloses a volume of aqueous phase with a thin membrane self-assembled by amphiphilic molecules, which is similar to liposome.[24~27] Some unique features, such as much larger surface area, higher compressibility, better biocompatibility than that of the polymeric micelles, and simultaneous encapsulation of hydrophilic and hydrophobic agents and so on, make polymeric vesicle applicable for drug delivery and bioimaging.[28-31] And that is why we adopt polymeric nanovesicle to encapsulate PFOB as UCA for anticipated high echo intensity and bioavailability. In this paper, an amphiphilic block copolymer, PEG-PDLLA, was developed to construct a novel self-assembled nanovesicle with low content of PFOB for in vitro and in vivo ultrasound imaging. These polymereic nanovesicles with low content of PFOB and good contrast –enhancing effect would have wide application as UCA for normal angiography and specific imaging of capillary-abundant organs or tissues (e.g. tumor).The main text of the article should appear here with headings as appropriate.

Experimental Section

Materials

Monomethoxy-ω-hydroxy polyethylene glycol [molecular weight (M.W.): 2,000 g/mol; PEG], PFOB (99%), stannous octoate [~95%; $Sn(Oct)_2$] and agarose were purchased from Sigma-Aldrich and used without further treatment. D, L- lactide (99%, Shenzhen Esun Industrial Co., Ltd, China) was recrystallized twice in anhydrous ethyl acetate and then vacuum-dried overnight. Polyvinyl alcohol (M.W.: 500 g/mol) was supplied by Guangdong Guanghua Chemical Factory Co., Ltd, China). Toluene (AR, Guangzhou Chemical Reagent Factory, China) was dehydrated by atmospheric distillation over calcium hydride (CaH_2) prior to use. All other regents are of analytic grade and dried or redistilled before the use.

Synthesis of PEG-PDLLA copolymer and poly(D,L-lactic acid) (PDLLA) homopolymer

PEG-PDLLA diblock copolymer was synthesized by ring-opening polymerization of D, L-lactide in the presence of $Sn(Oct)_2$ as a catalyst and PEG as a macroinitiator. Typically, 0.2 g of PEG was heated to 60 °C under vacuum for 2 hours to remove residual moisture. After cooled to room temperature, a drop of $Sn(Oct)_2$ was added to be dried and then mixed with 2 g of D, L-lactide in 20 mL of freshly distilled toluene under dry argon atmosphere. The mixture solution was magnetically stirred at 120 °C for 12 hours. Finally, the purified products were obtained by precipitation twice in anhydrous ether and dried under vacuum. Similarly, the PDLLA homopolymer as control was synthesized by benzyl alcohol-initiated ring-opening polymerization.

Characterization of PEG-PDLLA copolymer and PDLLA homopolymer

H-Nuclear magnetic resonance (^{1}H-NMR)

The chemical structure of PEG-PDLLA copolymer was determined by ^{1}H-NMR spectrum (Mercury-plus 300, Varian, USA) in deuterated chloroform ($CDCl_3$), and the PDLLA homopolymer's did in deuterated dimethyl sulfoxide (DMSO-*d*6).

Gel permeation chromatogram (GPC)

Both the M.W. of both PDLLA and PEG-PDLLA were determined from GPC [Waters Breeze, Waters, USA; eluent: tetrahydrofuran (THF); flow rate: 1.0 mL/minute; column calibration: polystyrene standards].

Compatibility test of PEG-PDLLA copolymer with PFOB

Predetermined volumes of PFOB (including 5, 10, 20 and 40 μL) and 20 mg of PDLLA or PEG-PDLLA were fully dissolved in chloroform ($CHCl_3$) and then kept volatilized in an open glass culture dish at ambient temperature to form a thin film. Subsequently, the residual PFOB on the surface of the thin film was washed away with pure water. The final film samples were obtained by drying at ambient temperature for two days.

Thermogravimetric analysis (TGA)

The thermogravimetric analyses of the thin film samples of PEG-PDLLA containing PFOB were performed on a Netzsch TG-209 instrument (Germany) under nitrogen gas. 13~18 mg of samples were heated from 30 to 200 °C at a rate of 10 °C/minute using alumina crucibles.

Differential scanning calorimetry (DSC)

The DSC analyses of the thin film samples of PEG-PDLLA containing PFOB were performed on a Perkin-Elmer Dsc-7 instrument (U.S.A) under nitrogen gas (flow rate: 10 mL/min-1). Typically, the heating or cooling stage for samples in aluminum pan were programmed as follows: ambient temperature increased to 100 °C at a rate of 20 °C/min. held for 3 min., and subsequently reduced to -30 °C at a rate of 20 °C/min., held for 1 min. to eliminate the heat history, and

finally increased to 100 °C at a rate of 5 °C/min.. The glass transition temperatures (T_g) were estimated as the peak values of the transition region in the second heating run.

Preparation of PEG-PDLLA nanovesicles

Blank and PFOB-loaded PEG-PDLLA nanovesicles were prepared by two-step ultrasonic emulsification as shown in Scheme 1. Typically, a predetermined volume of PFOB (0, 5, 10, 20 or 40 μL) and 20 mg of PEG-PDLLA were dissolved in 2 mL of $CHCl_3$, and then mixed with 0.2 mL of ultrapure water by ultrasonic emulsification (Vibra Cells, Sonics, U.S.A.). Subsequently, the resulting emulsion was fully dispersed again in 40 mL of ultrapure water under sonication, followed by rotary evaporation to remove $CHCl_3$. Standing for 30 minutes later, the supernatant was taken out to remove the unloaded PFOB, and then centrifuged at low temperature. After the removal of the supernatant containing blank nanovesicles, the remaining solution was diluted with ultrapure water to 2 mL.

Characterization of PEG-PDLLA nanovesicles

Dynamic light scattering (DLS)

The particle sizes of the obtained nanovesicles were determined using a Brookhaven BI-200 SM instrument (U.S.A.) under the following conditions: temperature-25 °C, detector angle-90°, and incident laser wavelength-623 nm. All reported sizes were based on the average number, and each particle size was given as the means of at least five runs.

Scheme 1 Self-assembly of PFOB-loaded PEG-PDLLA nanovesicles.

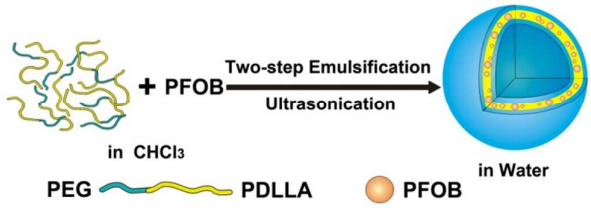

Transmission electron microscope (TEM)

The morphology of the obtained nanovesicles was recorded with a JEOL JEM-2010HR TEM (Japan). Samples were prepared by drying a dispersion of diluted nanovesicles solution on a copper grid coated with amorphous carbon. Afterwards, a droplet of phosphotungstic acid solution (1 wt.% in water) was added to stain the sample for 1 min., and then blotted with filter paper. The prepared sample was dried at room temperature before TEM observation.

In vitro ultrasound imaging

All operations were shown in Scheme 2.

Scheme 2 Preparation of agarose gel mold for *in vitro* ultrasonic imaging: (A) extracting the dissolved bubbles from the agarose solution using a 50 mL syringe; (B) inserting 15 mL centrifuge tubes to create the sample wells as cooled at 4 °C; (C) pouring the sample solution into the sample wells for *in vitro* ultrasonic imaging.

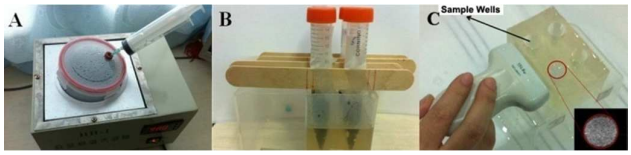

Agarose model

6 g of agarose and 200 mL of ultrapure water were added into a plastic container sealed with a rubber stopper (volume: 1000 mL) and heated to 80 °C for 30 min.. Afterwards, a portion of inner air was removed using a 50 mL syringe through the rubber stopper to make the agarose aqueous solution degassed. Once the obtained agarose solution was poured into a plastic cuboid container (volume: 500 mL), 15 mL plastic centrifuge tubes fixed with tongue depressors were immediately inserted into the solution and cooled at 4 °C for 1 hour. Thus, the desired agarose model without any bubble was obtained after the removal of the inserted centrifuge tubes.

In vitro ultrasound imaging

2 mL of nanovesicle solution was injected manually with a syringe into the sample well of agarose model. *In vitro* ultrasound imaging was performed and recorded using a Siemens Sequoia 512 clinical imaging system with a 15L8W-S probe in B-mode [frequency: 10 MHz; mechanical index (MI): 1.8; focus depth: 1.5 cm; gain: 0 and 10 db]. For the screenshots at 0 and 10 db of gain, all the gray values within the sample wells were measured by Image J software and given as the means of at least three runs ± standard deviation (SD).

In vivo ultrasound imaging

Subcutaneous imaging

Six-weeks-old BALB/c-nu mice (30~35 g) were purchased from the animal experiment center, Sun Yat-sen University. After anesthetized by intraperitoneal injection of 10% chloral hydrate, the mice body below the head was immersed in the water surface at 30 °C for ultrasonic observation. The local imaging under the skin was performed using a Siemens Sequoia 512 clinical imaging system with a 15L8W-S probe (frequency: 10 MHz; MI: 1.8; focus depth: 1.5 cm; gain: 0 db), and recorded before and after subcutaneous injection of 200 μL of the sample. The same dose of saline was used as negative control.

Intra-tumor imaging

Rat Walker-256 tumor cells was purchased from China Center for Type Culture Collection, Wuhan University. Four-week-old BALB/c-nu mice (male, 20~25 g) were purchased from the animal experiment center, Sun Yat-sen University. Each nude mouse was subcutaneously injected with 200 μL of Walker-256 tumor cell suspension (5×10^6 cells/mL) on the back, and fed for 3~4 weeks until the tumors reached a diameter of about 1.0 cm. The tumor-bearing mice were firstly anesthetized by intraperitoneal injection of 10% chloral hydrate, and immersed in the water at 30 °C except the head. Intra-tumor imaging was performed using a Siemens Sequoia 512 clinical imaging system with a 15L8W-S probe (frequency: 10 MHz; MI: 1.8;

focus depth: 1.5 cm; gain: 0 db), and recorded before and after intra-tumoral injection of 500 μL of the sample.

Blood pool imaging

Eight-week-old Wistar rats (male, 300 g) were purchased from the animal experiment center, Sun Yat-sen University. Prior to ultrasonic observation, these rats were anesthetized by intraperitoneal injection of 10% chloral hydrate and dehaired around the abdomen and chest using a depilatory cream. Blood pool imaging was performed using an Aloka α7 clinical imaging system with a 5412 probe (frequency: 10 MHz; focus depth: 2 cm; gain: 65 db). The corresponding ultrasonic tomograms of left ventricle, right kidney, and liver were recorded 20 seconds before and after intravenous injection of 700 μL of the mixed sample (containing 500 μL of the sample and 200 μL of saline) into the tail vein. In these images, the gray values were determined from the oval sampling frames located within the left ventricle, renal cortex and liver parenchyma by Image J software, and presented as the means of three runs ± SD.

Statistical analysis

Statistical analysis was performed using the SPSS 17.0 statistical package (SPSS, Chicago, U.S.A.). Differences in the imaging qualities between non- and contrast-enhanced groups were evaluated by t-test for the quantitative parametric data, considering $p < 0.05$ statistically significant.

Results and discussion

To PEG-PDLLA block copolymer, the M.W. of PDLLA was ~21,120 g/mol as determined by the signal intensities of -CH_2- in the repeating units of PEG block (chemical shift: ~3.6 ppm) and side -CH_3 in the repeating units of PDLLA block (chemical shift: ~1.5 ppm) in the ^{1}H-NMR spectrum. Given the M.W. of PEG, this result corresponded well with the number-average M.W. of PEG-PDLLA (23,475 g/mol) determined by GPC. So its M.W. ratio of hydrophilic units (PEG block) to hydrophobic units (PDLLA block) reached 10, which fully satisfied the requirement of forming polymeric vesicles.[32,33] As control, the M.W. of PDLLA homopolymer was also about 20,000 g/mol as determined by ^{1}H-NMR and GPC.

PFOB content

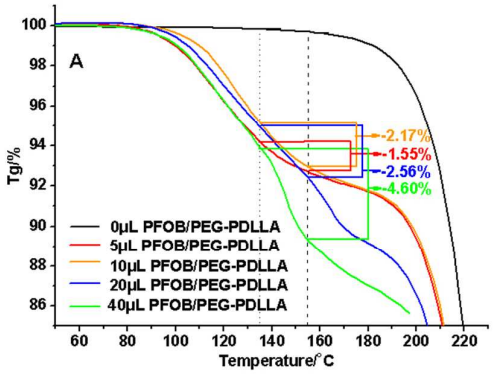

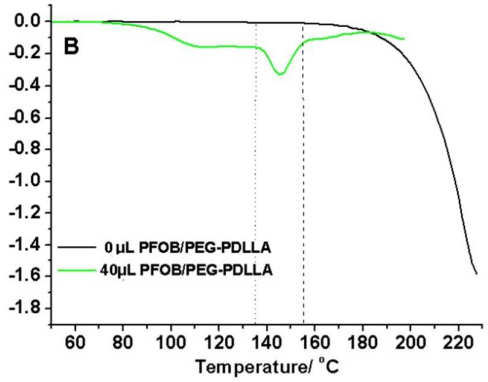

Figure 1 Thermogravimetric (A) and differential thermogravimetric curves (B) of the PEG-PDLLA vesicle solutions with different PFOB-loaded volumes (blank PEG-PDLLA vesicle as control).

The PFOB contents were firstly determined from the thermogravimetric curves of PFOB/PEG-PDLLA mixture film. As shown in Figure 1A, there was an obvious weight loss in the thermogravimetric curve over 80 °C, except the pure polymer sample. According to the differential thermogravimetric curves in Figure 1B, a gentle weight descent in the range from 80 to 110 °C can be ascribed to evaporation of residual water in the samples, while a drastic one over 190 °C can do to the thermolysis of PDLLA chain segments. Particularly, there was a sharp loss around PFOB b.p. in the range from 135.4 to 155.0 °C, suggesting the existence of PFOB in the samples. The accurate PFOB contents were calculated in this temperature range (see Table 1), which showed an obvious increase along with the PFOB feed: 4.60 wt.% for the 40 μL of PFOB feed was much higher than 1.55 wt.% for the 5 μL. However the loss is inevitable during the self-assembly of the amphiphilic PEG-PDLLA copolymer in aqueous solution, so that the real loading efficiency of PFOB in the polymeric devices is lower than the calculated PFOB content. This means that, only less than 4.60 % of PFOB can be loaded with the 40 μL of PFOB feed.

Table 1 Particle sizes and maximal PFOB loading efficiency of the PEG-PDLLA nanovesicles with different volumes of PFOB feed.

PEG-PDLLA Nanovesicle Samples	I	II	III	IV	V
PFOB Feed (μL)	0	5	10	20	40
Mean Particle Size (nm)	462.5	474.4	583.3	648.7	761.4
Maximal PFOB Loading Efficiency (%)	--	1.55	2.17	2.56	4.60

Compatibility of PFOB with PDLLA and PEG-PDLLA

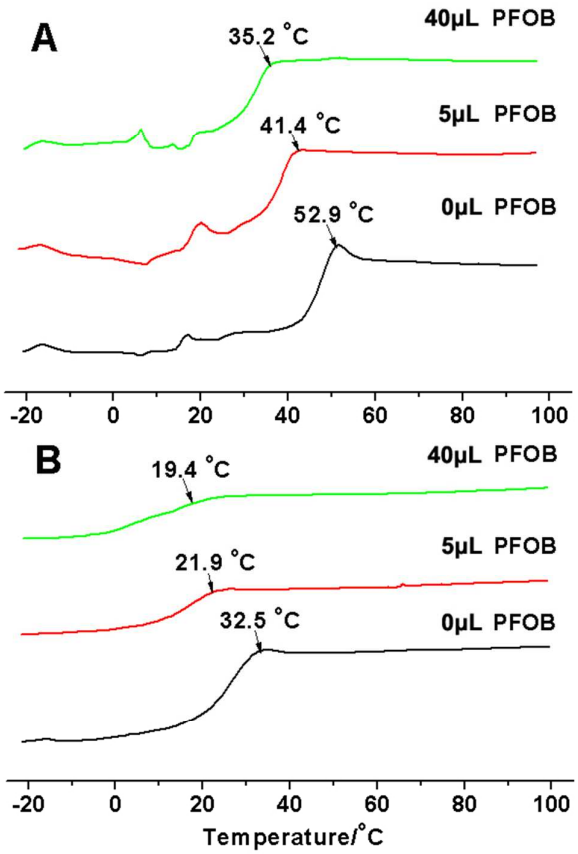

Figure 2 DSC curves of the mixtures of PFOB with PDLLA (A) and PEG-PDLLA (B).

In Figure 2, the pure PDLLA exhibited a sharp glass transition at 52.9 °C (T_g) that agrees with the previous reports.[34,35] After mixed with 5 and 40 μL of PFOB, the glass transition behaviors of PDLLA were still apparent, but both of the turning points were weakened and decreased to 41.4 °C and 35.2 °C, respectively. Obviously, the chain mobility of PDLLA might benefit from the addition of PFOB due to the excellent compatibility of hydrophobic PDLLA with PFOB.[34] PEG-PDLLA copolymer behaved well in almost the same thermal manner. The pure PEG-PDLLA exhibited a smooth glass transition at 32.5 °C (Tg) for the plasticization of PEG chain segments.[34,36] Once PFOB was mixed, its Tg decreased along with the increasing PFOB contents. Noticeably, the effect of PFOB on the Tg of PDLLA-PEG was greater than the one on PDLLA's: 11.5 °C: 10.6 °C as 5 μL of PFOB mixed; 17.7 °C: 13.1 °C as 40 μL of PFOB mixed. This suggested an excellent compatibility of PFOB with the PDLLA chain segments, which favored the encapsulation of PFOB into hydrophobic domains during the self-assembly of PEG-PDLLA.

Particle sizes and morphology

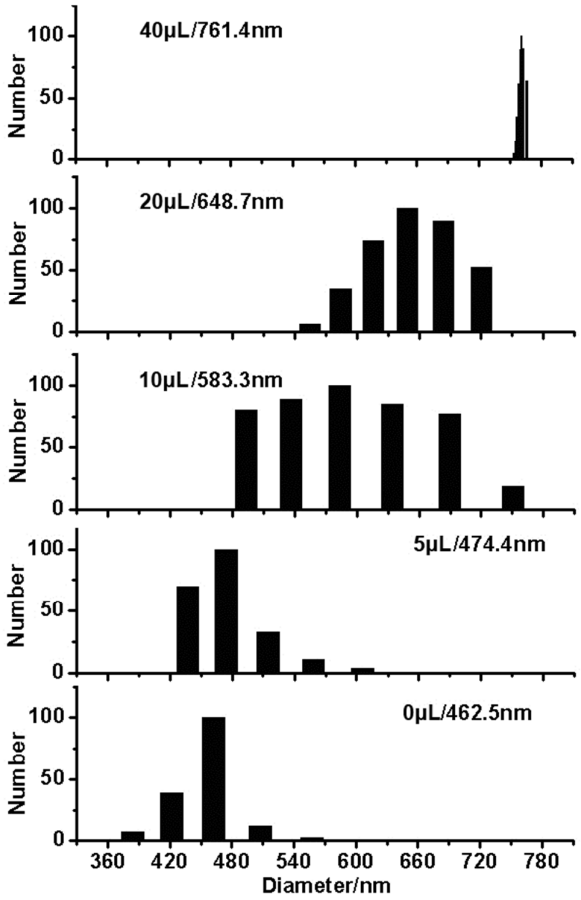

Figure 3 Particle-size distribution of PEG-PDLLA vesicles with different PFOB feeds.

As shown in Scheme 1, we prepared blank and PFOB-loaded PEG-PDLLA nanovesicles by two-step ultrasonic emulsification. Each of the obtained nanovesicles displayed a narrow distribution in particle sizes (see Figure 3), especially for the 40 μL-PFOB-feed sample. Their sizes gradually increased from 462.5 to 761.4 nm with the increase of PFOB feed (see Table 1). But as only a bit of PFOB (10 μL or less) fed, the sizes of resulting nanovesicles didn't increase much and were close to the blank nanovesicles'. A benefit of this size range was to ensure that these polymeric nanovesicles can enter tumor tissues through the gaps of vascular endothelium.[37]

Figure 4A illustrated some regular hollow spheres with about 26 nm of shell thickness, in which a rounded breach appeared on the surface of each individual nanoparticle. Particularly, many white dots, namely unstained PFOB droplets, spread throughout the vesicular shell (see Figure 4B). This indicated that the visible spherical shells were hydrophobic and sure to encapsulate PFOB, in good accord with the configuration of polymeric nanoveiscle in Scheme 1. In addition, these hollow spheres had similar particle sizes to that of blank nanovesicles, but not the 40 μL-PFOB-feed nanovesicle in Figure 3. This could be explained that, the nanovesicle sample was fully

diluted to keep the crude configuration of single vesicle prior to TEM observation, but stayed concentrated in the particle size determination, so that the particle size of PFOB-loaded nanovesicles might increase unavoidably as aggregation.

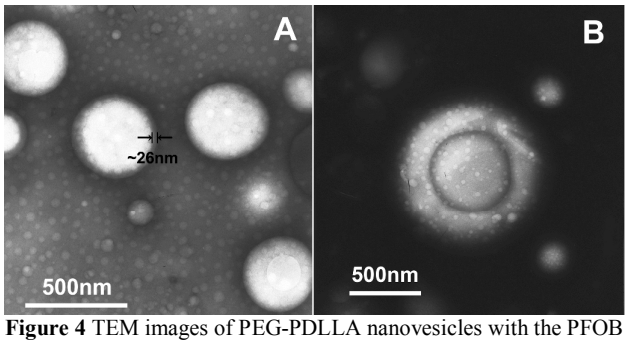

Figure 4 TEM images of PEG-PDLLA nanovesicles with the PFOB feed of 40 μL.

***In vitro* ultrasound imaging**

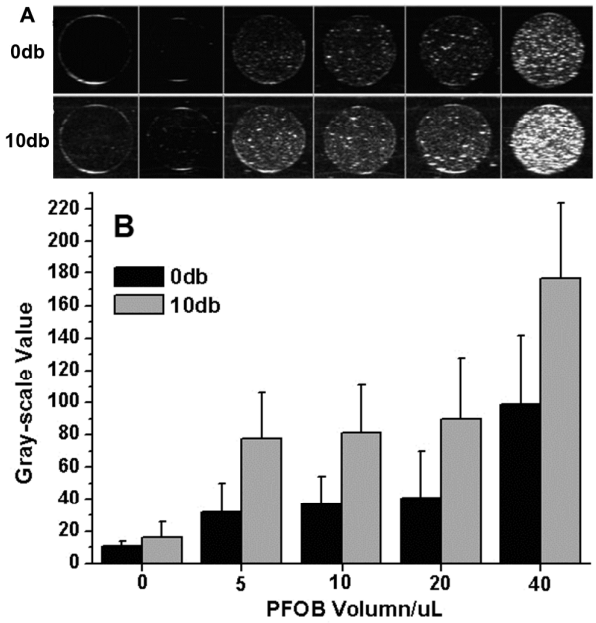

Figure 5 *In vitro* ultrasound imaging of the PEG-PDLLA vesicle solutions with different PFOB-loaded volumes at the gain of 0 db or 10 db (A) and the corresponding gray-scale values (B).

The *in vitro* and *in vivo* ultrasound imaging results further verified the high efficiency of PEG-PDLLA self-assembled nanovesicles with low content of PFOB. From the ultrasonic images of different PFOB-feed nanovesicle samples, it clearly showed that the PEG-PDLLA nanovesicles without PFOB appeared to be visible in aqueous solution and their brightness are enhanced with the increase of PFOB-feed (see Figure 5A). Particularly in the circular sample frame, a few bright spots originated from large particles appeared on the homogeneously brightened background without any gain. This was well consistent with the partial aggregation in concentrated nanovesicle solution. Figure 5B displayed the corresponding mean gray values. In the statistical analysis of completely randomized block designs, the difference in mean gray values among different PFOB-feed nanovesicle groups was statistically significant (p=0.013). And the statistical tests of least significant difference (LSD) on any two groups indicated that: to 40 μL-PFOB-feed group, its p values ranged from 0.002 to 0.017 showing statistically significant difference; between 0 and 20 μL-PFOB-feed groups, the p value was 0.047 also showing statistically significant difference; however, compared among the rest groups, their p values ranged from 0.069 to 0.838, showing no significant statistical difference. So the PEG-PDLLA nanovesicles presented outstanding contrast-enhanced effect only if the PFOB feed reached 20μL and more. In detail, the mean gray value greatly increased from 41 to 99 as the PFOB feed increased from 20 μL to 40 μL at 0 db of gain, and does also from 90 to 177 at 10db of gain.

***In vivo* ultrasound imaging**

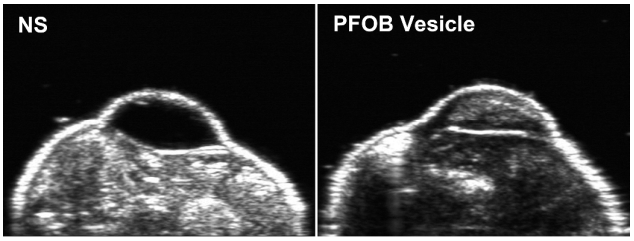

Figure 6 Ultrasound imaging after subcutaneous injection of the 40μL-PFOB-feed PEG-PDLLA nanovesicle solution [normal saline (NS) as control].

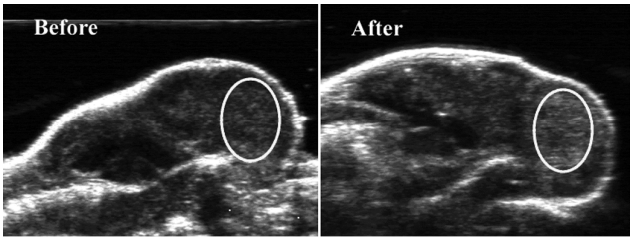

Figure 7 Ultrasound imaging of the 40μL-PFOB-feed PEG-PDLLA nanovesicle solution before (left) and after intratumor injection (right).

In vivo experiments involved subcutaneous, intratumor, and blood pool imaging. After first subcutaneous injection, nanovesicle solution localized between skin and subcutaneous fascia layer, and appeared as hummocky bulge (see Figure 6). The brightness was homogeneously and obviously increased with a sprinkling of bright spots, similar to the *in vitro* ultrasound images. On the contrary, normal saline does behaved without a trace of gain. It indicated that these PFOB-loaded nanovesicles exerted an excellent echo-enhanced effect. Similarly, a local swell of tumor occurred after intratumor

injection of the nanovesicle solution (see Figure 7). In the sample frame, homogeneous and tiny spotty echo was observed, indicating that the echo intensity was enhanced.

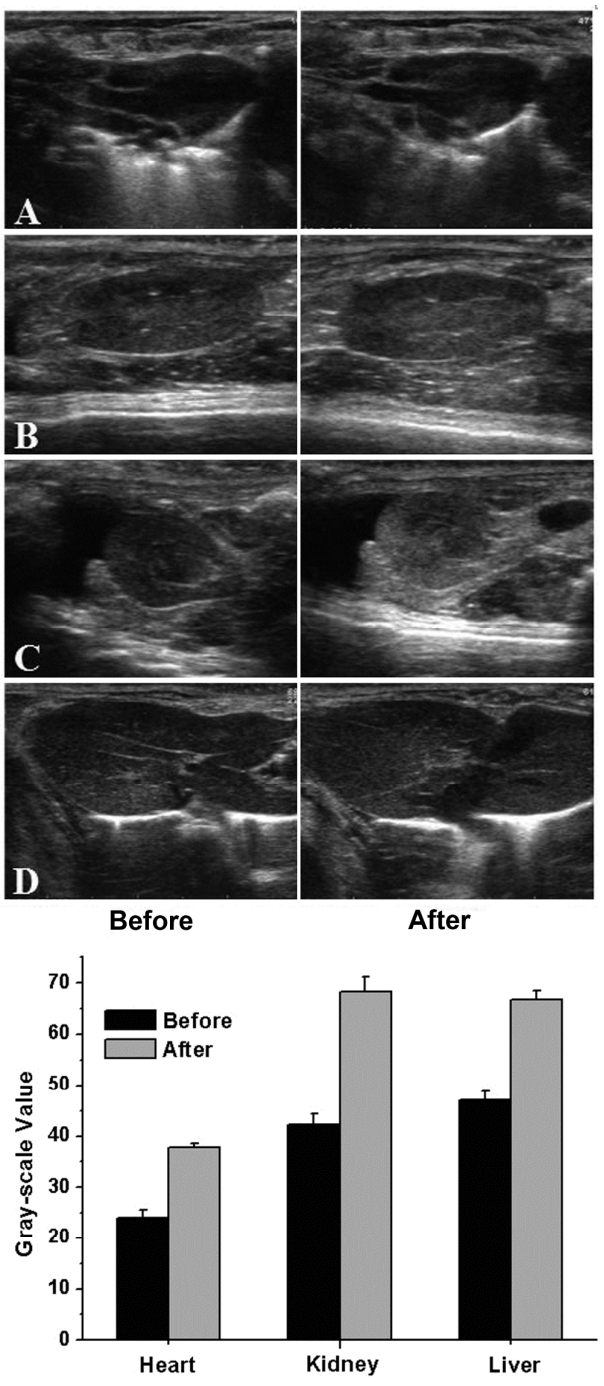

Figure 8 Ultrasound imaging of the 40μL-PFOB-feed PEG-PDLLA nanovesicle solution before (left) and after intravenous injection (right) into different organs of normal rats, and the corresponding gray-scale values. (A: heart; B: vertical axis of the right kidney; C: horizontal axis of the right kidney; D: liver)

Several representative organs, including heart, liver, and kidney, were observed for the blood pool imaging. The ultrasound images before and after tail intravenous injection of 40 μL-PFOB-feed PEG-PDLLA nanovesicle solution were recorded in Figure 8A. All the cavities within these organs, especially for the horizontal axis of the right kidney, had slight and homogenous enhancement without any highlighted spot. Correspondingly, all the post-injection mean gray values increased in Figure 8B. Their difference in imaging qualities was analyzed by t-test, and considered to be statistically significant ($p= 0.031$). It revealed that these nanovesicles featured contrast-enhanced effect for the blood pool ultrasound imaging. According to Equation 1, this contrast effect of the PFOB-loaded nanovesicles was originated from the particle concentration (n), geometric dimensioning (V and r) and material property (γ_c and γ_d). In fact, the injected nanovesicle solution was overly diluted in blood circulation, resulting in a low n value and no large aggregation (namely no highlight in intracavities). On the other hand, PFOB, as a common and excellent liquid contrast agent, was loaded in tiny amounts (the maximum loading efficiency: 4.60% for the 40 μL of feed as shown in Table). These polymeric vesicles with the size of about 500 nm were much smaller than microbubbles but achieved good contrast-enhanced imaging. This could be only ascribed to their special structure, in which the PFOB was uniformly distributed throughout the hydrophobic shell of the nanovesicles (see Figure 4B). Based on the good compatibility of PFOB with PDLLA block, the physical properties of the nanovesicles, including compressibility (namely γ_c term) and shell density (namely γd term) would be dramatically improved compared to other PFOB nanoparticles with the same feed. As shown in Figure 8, the PFOB-loaded nanovesicles as ultrasound scatterer greatly enhanced the echo intensity and become available for in vivo imaging, especially for blood pool imaging. Furthermore, the nano-scale particle size would make credible intratumor imaging by intravenous injection possible. And the low content of PFOB could also avoid some potential adverse reactions.

Prior to *in vitro* and *in vivo* ultrasound imaging, hollow PFOB sphere similar to the PFOB-loaded polymeric nanovesicle is used as a calculation model for theoretical imaging evaluation. In general, the contrast-enhanced effect of UCA crucially relies on its backscatter intensity (I) as defined by the following equation[3]:

$$I / I_0 \sim \frac{1}{9} nV[k^4 r^6 (\gamma_c + \gamma_d \cos\theta)^2 / d^2] \qquad \textbf{Equation 1}$$

Here I_0 is the incident intensity, n is the number density of scattering particles, V is the scattering volume, k is the number of incident wave (the ultrasound emission frequency), r is the radius of the particle, γ_c is the compressibility term [$\gamma_c=(\kappa_s-\kappa_m)/\kappa_m$, where κ_s and κ_m are the compressibilities of scatterer and ambient medium, respectively], γ_d is the density term [$\gamma_d=(3\rho_s-3\rho_m)/(2\rho_s+\rho_m)$, where ρ_s and ρ_m are the densities of scatterer and ambient medium, respectively], θ is the scattering angle (180° for backscattering), and d is the distance from the scatterers.

In a fixed ultrasound field, I depends mainly on r, γ_c, and γ_d term of UCA. Particularly, I is in direct proportion with the

sixth power of *r*. This explains why microbubbles are much better than nano-sized UCAs in ultrasound imaging. So the *r* term of UCA is firstly discussed under different situations. As a key calculation model of UCA (see Scheme 3), hollow PFOB sphere is defined with the diameter (d_h) of 500 nm and the shell thickness of 26 nm which are resulted from the nanovesicles in Figure 4.

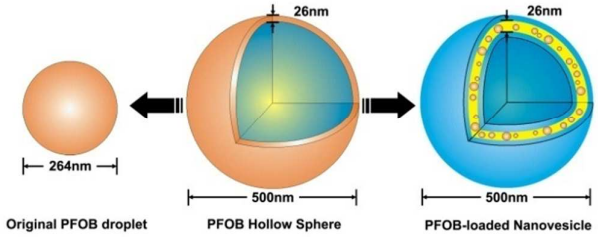

Scheme 3 Original PFOB nanodroplet, hollow sphere, and PFOB-loaded nanovesicle with the same volume as the calculation models of backscatter intensity.

(1) If the external volumes of both hollow and solid PFOB sphere are equal, their ratio of mass (R_m) is calculated as:

$$\boldsymbol{R_m}(h{:}s)=\frac{\rho V_h}{\rho V_s}=\frac{\frac{4}{3}\pi(\frac{d_h}{2})^3-\frac{4}{3}\pi(\frac{d_h-26}{2})^3}{\frac{4}{3}\pi(\frac{d_h}{2})^3}=\frac{500^3-474^3}{500^3}=0.15$$

Although *r* is equal, the need of PFOB mass in the hollow sphere is only 15% of that in the solid sphere.

(2) If the PFOB volumes of both original and hollow PFOB sphere are equal, their ratio of diameter (R_d) is calculated as:

$$\frac{4}{3}\pi(\frac{d_h}{2})^3-\frac{4}{3}\pi(\frac{d_h-26}{2})^3=\frac{4}{3}\pi(\frac{d_o}{2})^3 \quad \Rightarrow d_o\approx 264\text{nm}$$

$$\Rightarrow \boldsymbol{R_d}(h{:}o)=\frac{d_h}{d_o}=\frac{500}{264}=1.89$$

Where d_o is the diameter of the original PFOB sphere. Although both the volume and mass of PFOB are the same, the diameter of the hollow sphere is almost double of that of the solid sphere. It means that, its *I* value would be 64 times more than that of the solid sphere regardless of γ_c and γ_d term. Thus, at least from the perspectives of mass need and r, the hollow sphere is much better than the solid sphere with the same material in *I* for UCA application.

However, hollow PFOB sphere unlikely exists owing to the weak intermolecular forces inside the PFOB liquid.[23] In contrast, the PFOB-loaded and PEG-PDLLA self-assembled nanovesicle with the same geometrical configuration of the hollow PFOB sphere is thermodynamically stable in aqueous solution. According to the 40 μL-PFOB-feed nanoveislce in Figure 4A, this polymeric model is set with the diameter of 500 nm, the shell thickness of 26 nm, and the scattering shell comprised of hydrophobic PDLLA and PFOB (content: 4.60 wt.%). For such a spherical particles smaller than the wavelength of incident ultrasound, its I depends mainly on the compressibility (γ_c term) and the difference between the density of scatterer and ambient medium (γ_d term) except for r term. If the density of PDLLA is assumed to be 1.20 g/cm^3 with reference to PLA24 (M.W.: 24 kDa) mentioned in a previous report[38], the density of the nanovesicle shell and whole nanovesicle (ρ_s) are calculated to be 1.24 g/cm^3 (PFOB: 1.92 g/cm^3) and 1.07 g/cm^3, respectively. So the γ_d term is 0.06 [ρ_m (water): 1.00 g/cm^3], much less than that of pure PFOB droplet (0.57). But given the negative suffixal term—cosθ (θ=180° for backscattering), the lower γ_d term of PFOB-loaded nanovesicle will actually increase the value of *I*.

And its γ_c term is also more than that of the PFOB droplet, since the intertwined PDLLA chains make nanovesicle shell elastic and resistant to pressure, and thus exhibits much higher compressibility than PFOB and water.[3] According to Equation 2[39], the volume compressibility κ is defined as the reciprocal of adiabatic compressibility (β), namely the product of the scatter density (ρ_s) and the square of ultrasound velocity (*v*) shown as follow:

$$\kappa=v^2\rho_s \qquad \textbf{Equation 2}$$

Hereinto, the *v* of PDLLA, PFOB and water are 2262.5 (25 °C)[38], 631.8 (21.2 °C)[40] and 1496.7 m/s (25 °C)[38], respectively. If the different temperature of water and the effect of the little PFOB in PDLLA nanovesicle shell on *v* are neglected, we can calculate the value of γ_c: 1.44 for the PFOB-loaded PEG-PDLLA nanovesicle; -0.66 for the pure PFOB droplet. Therefore compared to the other nano-sized configurations of pure PFOB, the polymeric nanovesicle with the low content of PFOB is quite helpful in enhancing its own ultrasound backscatter intensity.

Conclusions

Amphiphilic block copolymer, PEG-PDLLA was utilized to construct PFOB-loaded nanoveislces with hollow spherical structure by self-assembly. Although at very low content of PFOB, the echo intensity of the nanoveislce was greatly enhanced and much exceeded other PFOB nanoparticles with same feed or volume. Uniformly distributed PFOB could integrate well with the hydrophobic PDLLA blocks to improve the compressibility and shell density of the nanovesicles as ultrasound scatterer. Besides the outstanding local imaging, these overly diluted nanovesicles also show quite a good contrast-enhanced effect for blood pool imaging. Therefore, this PFOB-loaded polymeric nanovesicle is applicable as UCA for in vivo imaging, including normal angiography and specific imaging of capillary-abundant organs or tissues (e.g. tumor).

Live subject statement

All animal experiments were performed under the protocols approved by the Animal Care and Use Committee of Sun Yat-Sen University, and in accordance with the Guide for the Care and Use of Laboratory Animals published by the National Institutes. And all animals involved in this research were raised and breed followed the guidelines of Animal Husbandry Department of Guangdong, P.R.China. All efforts were made to minimize suffering.

Acknowledgements

This work was supported by National Basic Research Program of China (2015CB755500), National Natural Science Foundation of China (51225305, U1401242, 81430038, and 81271577), Natural

Science Foundation of the Guangdong Province (2014A030312018), and Guangdong Innovative and Entrepreneurial Research Team Program (2013S086).

Notes and references

1 A. L. Klibanov, *Bioconjugate Chem.*, 2005, **16**, 9-17.
2 J. D. Lathia, L. Leodore and M. A. Wheatley, *Ultrasonics*, 2004, **42**, 763–768.
3 E. G. Schutt, D. H. Klein, R. M. Mattrey and J. G. Riess, *Angew. Chem. Int. Ed.*, 2003, **42**, 3218 – 3235.
4 A. P. Miller and N. C. Nanda, *Ultrasound Med. Biol.*, 2004, **30**, 425–434.
5 S. Tinkov, R. Bekeredjian, G. Winter and C. Coester, *Journal of Pharmaceutical Sciences*, 2009, **98**, 1935-1961.
6 M. Néstor, N. E. Kei, N. M. Guadalupe, M. S. Elisa, G. Adriana and Q. David, *Ultrasonics*, 2011, **51**, 839–845.
7 Y. Wang, X. Li, Y. Zhou, P. Y. Huang and Y. H. Xu, *International Journal of Pharmaceutics*, 2010, **384**, 148-153.
8 E. Pisani, N. Tsapis, J. Paris, V. Nicolas, L. Cattel and E. Fattal, *Langmuir*, 2006, **22**, 4397-4402.
9 J. N. Marsh, K. C. Partlow, D. R. Abendschein, M. J. Scott, G. M. Lanza and S. A. Wickline, *Ultrasound Med Biol.*, 2007, **33**, 950–958.
10 E. Pisani, N. Tsapis, B. Galaz, M. Santin, R. Berti, N. Taulier, E. Kurtisovski, O. Lucidarme, M. Ourevitch, B. T. Doan, J. C. Beloeil, B. Gillet, W. Urbach, S. L. Bridal and E. Fattal, *Adv. Funct. Mater.*, 2008, **18**, 2963–2971.
11 J. Y. Fang, C. F. Hung, S. C. Hua and T. L. Hwang, *Ultrasonics*, 2009, **49**, 39–46.
12 R. Díaz-López, N. Tsapis, M. Santin, S. L. Bridal, V. Nicolas, D. Jaillard, D. Libong, P. Chaminade, V. Marsaud, C. Vauthier and E. Fattal, *Biomaterials*, 2010, **31**, 1723–1731.
13 Z. G. Gao, A. M. Kennedy, D. A. Christensen and N. Y. Rapoport, *Ultrasonics*, 2008, **48**, 260–270.
14 N. Rapoport, A. M. Kennedy, J. E. Shea, C. L. Scaife and K. Nam, *Journal of Controlled Release*, 2009, **138**, 268-276.
15 N. Rapoport, A. M. Kennedy, J. E. Shea, C. L. Scaife and K. Nam, *Molecular Pharmaceutics*, 2010, **7**, 22–31.
16 K. Shiraishi, R. Endoh, H. Furuhata, M. Nishihara, R. Suzuki, K. Maruyama, Y. Oda, J. Jo, Y. Tabata, J. Yamamoto and M. Yokoyama, *International Journal of Pharmaceutics*, 2011, **421**, 379– 387.
17 N. Rapoport, K. Nam, R. Gupta, Z. G. Gao, P. Mohan, A. Payne, N. Todd, X. Liu, T. Kim, J. Shea, C. Scaife, D. L. Parker, E. Jeong and A. M. Kennedy, *Journal of Controlled Release*, 2011, **153**, 4-15.
18 S. M. Moghimi, A. C. Hunter and J. C. Murray, *Pharmacol Rev.*, 2001, **53**, 283–318.
19 R. Savić, L. B. Luo, A. Eisenberg and D. Maysinger, *Science*, 2003, **300**, 615-618.
20 R. F. Mattery, F. W. Scheible, B. B. Gosink, G. R. Leopold, D. M. Long and C. B. Higgins, *Radiology*, 1982, **145**, 759-762
21 G. M. Lanza, K. D. Wallace, M. J. Scott, W. P. Cacheris, D. R. Abendschein, D. H. Christy, A. M. Sharkey, J. G. Miller, P. J. Gaffney and S. A. Wickline, *Circulation*, 1996, **94**, 3334-3340.
22 K. C. Lowe, *Clinical Hemorheology*, 1992, **12**, 141-156.
23 D. M. Lemal, *J. Org. Chem.*, 2004, **69**, 1-11.
24 H. W. Shen and A. Eisenberg, *Angew. Chem. Int. Ed.*, 2000, **39**, 3310-3312.
25 D. E. Discher and A. Eisenberg, *Science*, 2002, **297**, 967-973.
26 M. Antonietti and S. Förster, *Advanced Materials*, 2003, **15**, 1323-1333.
27 P. L. Luisi, T. P. D. Souza and P. Stano, *J. Phys. Chem. B*, 2008, **112**, 14655–14664.
28 J. Z. Du, L. Fan and Q. M. Liu, *Macromolecules*, 2012, **45**, 8275–8283.
29 O. K. Nag, C. S. Lim, B. L. Nguyen, B. Kim, J. Jang, J. H. Han, B. R. Cho and H. Y. Woo, *J. Mater. Chem.*, 2012, **22**, 1977–1984.
30 T. B. Ren, Q. M. Liu, H. Lu, H. M. Liu, X. Zhang, J. Z. Du, *J. Mater. Chem.*, 2012, **22**, 12329–12338.
31 S. W. Kang, Y. Li, J. H. Park and D. S. Lee, *Polymer*, 2013, **54**, 102-110.
32 F. H. Meng, C. Hiemstra, G. H. M. Engbers and J. Feijen, *Biomacromolecules*, 2003, **36**, 3004-3006.
33 P. L. Soo and A. Eisenberg, *J. Polym. Sci. Part B: Polym. Phys.*, 2004, **42**, 923-938.
34 O. Martin and L. Avérous, *Polymer*, 2001, **42**, 6209-6219.
35 R. Steendam, M. J. V. Steenbergen, W. E. Hennink, H. W. Frijlink and C. F. Lerk, *Journal of Controlled Release*, 2001, **70**, 71–82.
36 A. Lucke, J. Teβmar, E. Schnell, G. Schmeer and A. G. Pferich, *Biomaterials*, 2000, **21**, 2361-2370.
37 S. K. Hobbs, W. L. Monsky, F. Yuan, W. G. Roberts, L. Griffith, V. P. Torchilin and R. K. Jain, *Proc. Natl. Acad. Sci. USA*, 1998, 95, 4607–4612.
38 N. G. Parker, M. L. Mather, S. P. Morgan and M. J. W. Povey, *Biomedical Materials*, 2010, **5**, 055004.
39 T. Hianik, M. Haburcák, K. Lohner, E. Prenner, F. Paltauf and A. Hermetter, *Colloids and Surfaces A: Physicochemical and Engineering Aspects*, 1998, **139**, 189–197.
40 C. S. Hall, G. M. Lanza, J. H. Rose, R. J. Kaufmann, R. W. Fuhrhop, S. H. Handley, K. R. Waters, J. G. Miller and S. A. Wickline, *IEEE Transactions on Ultrasonics, Ferroelectrics, and Frequency control*, 2000, **47(1)**, 75-84.